

A SIMPLE STRUCTURED MULTIBAND TERAHERTZ METAMATERIAL ABSORBER WITH A HIGH Q FACTOR

ENOSTAVNO STRUKTURIRANI VEČ PASOVNI TERAHERČNI METAMATERIAL ZA ABSORBERJE Z VISOKIM Q FAKTORJEM

S. Deepa Nivethika

Vellore Institute of Technology University, Chennai – 600127

Prejem rokopisa – received: 2023-11-07; sprejem za objavo – accepted for publication: 2024-02-27

doi:10.17222/mit.2023.1040

A terahertz Eight-/Nine-/Twelve-/Fourteen-/Sixteen-Band Metamaterial Absorber (MMA) for sensing applications is built and simulated. The substrate is sandwiched between the bottom ground plane and the top patch structure of this primitive MMA. The top patch is made up of two concentric circular ring resonators. This structure generates a multiple number of multi bands without utilising stacked layers, multiple resonators, or overlapping in a single unit cell by altering the radius of the top patch structure within the shorter frequency range of 0.8 THz to 1.2 THz. The polarisation and angle insensitivity properties are investigated by shifting the angle values from 0 to 90 degrees. To learn about the inside mechanism of the planned structure, the magnetic field distribution, electric field distribution and surface current distribution plots are explained. For the sixteen-band MMA, the Q-Factor and full width half maximum are also determined. This proposed MMA will be used in biosensing applications, sensors and wireless communications.

Keywords: metamaterial, absorber, multiband, terahertz, Q-factor

Povzetek: avtor tega članka je zgradil in simuliral teraheerčni osem, devet, dvanajst, štirinajst in šestnajst pasovni absorberski metamaterial (MMA; angl: Metamaterial Absorber) za senzorje. Avtor je substrat kot sendvič namestil med spodnjo osnovno ploščo in vrhno plastjo te primitivne MMA strukture. Vrhna plast je bila izdelana iz dveh koncentričnih resonatorskih Cu obročev. Ta struktura generira večkratno število večpasovnosti, ne da bi zato uporabili zlog plasti, večvrstne resonatorje ali prekrivanje v enojni celici s spreminjanjem polmera zgornje strukture znotraj krajšega frekvenčnega območja od 0,8 THz do 1,2 THz. Avtor je ugotavljal, s spreminjanjem kota med 0 in 90 stopinjami, polarizacijo in lastnosti kotne neobčutljivosti. Spoznal in razložil je notranji mehanizem večplastne planarne strukture, porazdelitev magnetnega polja, porazdelitev električnega polja in potek površinskih tokov. Za šestnajst pasovni MMA je določil Q-Faktor in polno širino polovičnega maksimuma. Ta predlagani MMA bodo uporabili za biosenzorske aplikacije ter senzorje za brezžične komunikacije.

Ključne besede: metamaterial, absorber, večpasovnost, terahertz (THz), Q-faktor

1 INTRODUCTION

The last section of the electromagnetic field that needs to be examined is the terahertz wave (THz), which ranges from 0.1 to 10 THz. THz ray absorbing in atomic and biomolecular platforms is driven by the stimulating of intrinsic and inter-molecular movement, which include weakly linked molecules with bonds composed of hydrogen along with weak relations that involve van der Waals forces, which is important for a compound and biological molecules detection due to its location within infrared rays and microwave frequencies.^{1,2} Some compounds, such as illegal substances,³ antibacterial medications,⁴ herbicides,⁵ peptides,⁶ organisms that have been genetically modified,⁷ melamine,⁸ which and other dangerous remains,⁹ have been found as a result of absorption by identification through pounding powder samples into the pellets. Though, this kind of approach is best suited for investigating the possibility of THz detection, rather than analysing tiny amounts.

Metamaterials (MMs), which are the periodic engineered electromagnetic media- with a dimension level lower than a wavelength of the stimuli from the outside that exhibit features that are absent in nature.¹⁰ They were originally developed to achieve intriguing features like negative refractive index and invisibility.¹¹ The growth of MM study in the last 20 years has focused on multiple topics that were highlighted in certain reviews, among them all-dielectric MMs, adaptable MMs, versatile MMs, meta components, graphite MMs, adjustable MMs, and the meta surfaces. THz metamaterials, initially presented by Prof. Xiang Zhang's team,¹² have sparked widespread attention and are currently a hot topic in THz research and development, involving MM modulators, MM polarizers, THz wave generators, THz wave absorbers, and compression imaging.¹³

It is significant to note that, the purpose of this approach is not to improve a single aspect of the MMA, but rather to retain high absorbance at incident angles of both TM and TE polarisation in an identified range of THz frequencies. In this paper we offer an ultra-thin polarisation and incidence-angle-insensitive sixteen-band MMA. In the following sections, the relevant resonance

*Corresponding author's e-mail:
deepanivethika.s@vit.ac.in (S. Deepa Nivethika)

frequencies and absorption rate are discussed in graphs and tabulation forms. For the sixteen-band MMA, a higher Q factor can be offered. Metallic symmetrical circular ring resonators with compact and ultra-thin features can be offered in a unique shape. For both the TE as well as TM modes, the proposed metamaterial absorber exhibits virtually perfect absorption over a wide angle of incidence, up to 90°. In spite of its superior performance, this ultra-thin absorber is suitable for a wide range of applications, including spacecraft radar systems, concealed imaging, and electromagnetic disturbance reduction. Surface currents and electromagnetic field distributions are also examined in this paper to better understand the resonance mechanism. This research demonstrates that the suggested absorber can retain a high level of absorbance even at large incidence and polarisation angles.

2 STRUCTURE AND DESIGN

The proposed structure design, simulation and analysis is made using CST (computer simulation technology) Microwave Studio Software. Different developing stages of the MMA are shown in **Figures 1a** to **1c** and the 3-d view is shown in **1d**. This polarization-insensitive structure consists of three layers. The polyimide substrate is placed in between the two copper layers. The dielectric constant value (ϵ_r) of the polyimide is 3.5 and the electric tangent ($\tan \delta$) is 0.0027. The thickness of the substrate is 0.125 mm and the thickness of the ground plane is 0.001 mm. The conductivity of the copper is $\sigma = 5.8 \times 10^7$ S/m.¹⁴

Table 1: Parameters and dimensions of the MMA

Parameters	Dimensions (mm)
Length and Width of the substrate and ground plane (L×W)	(0.25×0.25)
R1, R2, R3, R4	0.06, 0.14, 0.16, 0.24
Thickness of the substrate	0.125 mm
Thickness of the ground plane	0.001 mm

The top patch consists of two concentric circular resonator structure, which is a very simple and easy structure. R1, R2, R3, R4 represented the radius value of the inner and outer circular resonators. And the length and width of the ground plane and substrate layer is the same. The corresponding dimensions are shown in **Table 1** and marked in **Figure 1d**.

2.1 Boundary Conditions and Absorption Rate of MMA

The unit-cell periodic boundary rule is used in both the x and y directions, besides the z free boundary situation, as shown in **Figure 2**. The simulation system is used to calculate the variables for angular frequency (ω), absorbance (abs), reflections (ref), and transmittance

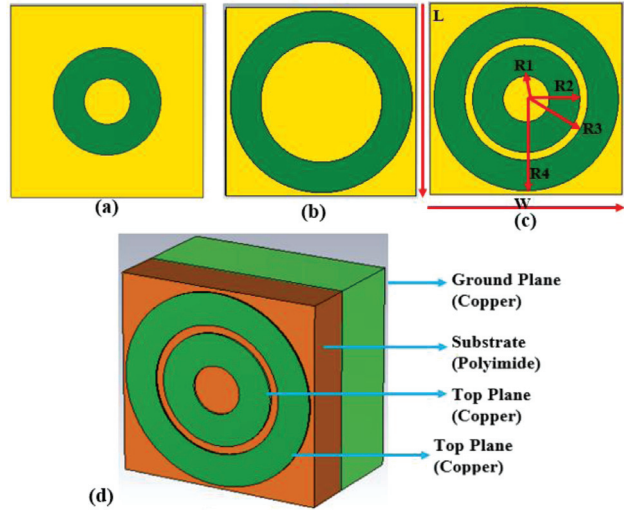


Figure 1: Different developing stages of the MMA: a) inner circle only, b) outer circle only, c) both inner and outer circle- polyimide in yellow, copper in green, d) perspective view of the MMA (3-layers)

(tra). The formula $Abs(\omega) = 1 - Ref(\omega) - Tra(\omega)$ is used to determine the absorption. The spectrum of the transmission confirms the null reception due to the existence of a thick, conductive, ground copper layer that is higher than its skin depth (δ). As a consequence, the absorbance is determined only by the reflected component. Because the designed structure produces improved reflections in the suitable bands, absorption is improved. The absorption coefficient will be one if the impedance is appropriately matched with open space.

If both the inner and outer rings are present it means the proposed structure resonated at sixteen different frequencies, i.e., 0.80 THz, 0.83 THz, 0.876 THz, 0.895 THz, 0.92 THz, 0.93 THz, 0.957 THz, 0.962 THz, 0.988 THz, 0.997 THz, 1.02 THz, 1.04 THz, 1.09 THz, 1.112 THz, 1.137 THz and 1.154 THz, with absorption rates of 93 %, 86 %, 99.6 %, 86.5 %, 94 %, 93 %, 98 %, 96 %, 97 %, 95 %, 98 %, 96 %, 91 %, 91.2 %, 80 % and 99 %, respectively, which is shown in **Figure 3c**. Also, chang-

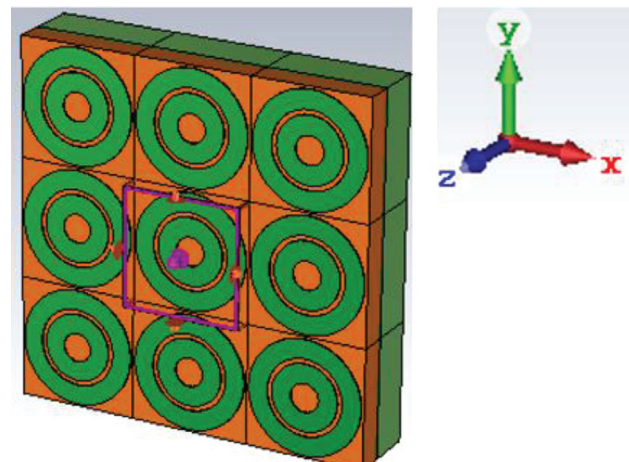


Figure 2 Unit-cell boundary along with axis

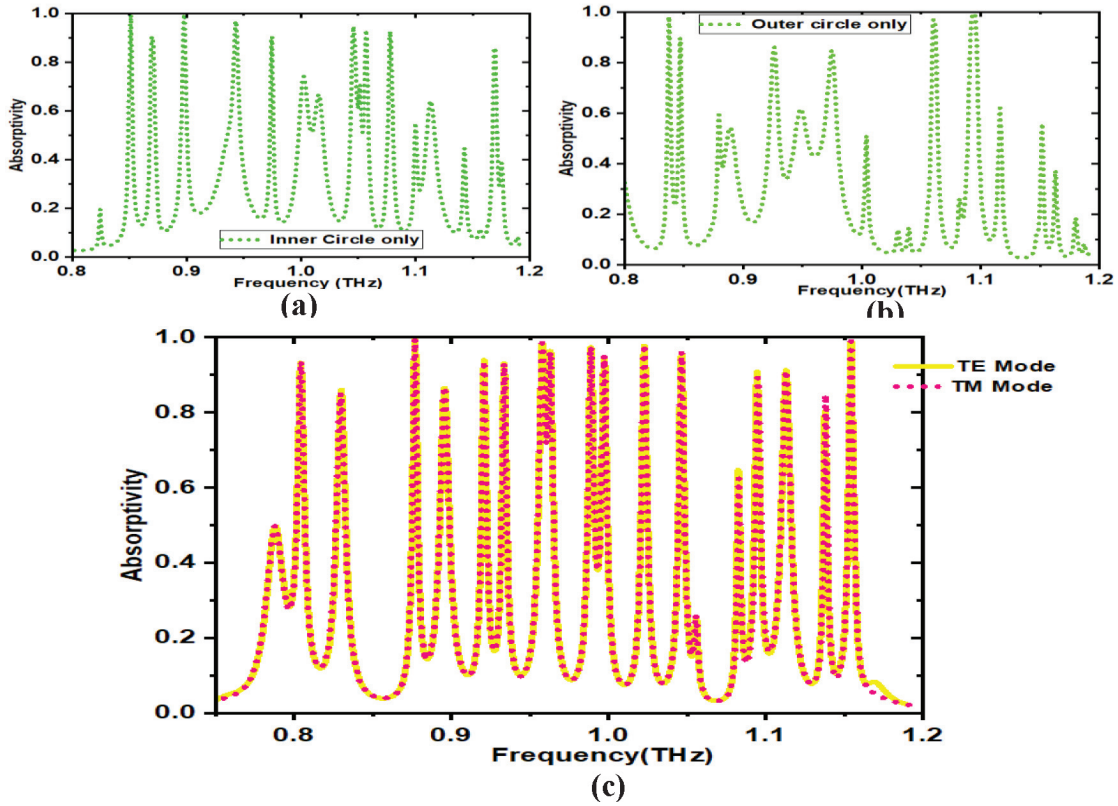


Figure 3: a) Inner circle only presents 10 resonance bands, b) outer circle only presents 6 resonance bands, c) both inner and outer patch present 16 resonance bands for both TE and TM mode

ing the top-patch parameter values gives the Eight-/Nine-/Twelve-/Fourteen bands which are explained in the upcoming sections (i.e., the parameter study).

3 RESULTS AND DISCUSSION

3.1 Absorption Rate Characteristics

The different developing stages of the MMA are shown in **Figures 1a to 1c** and the corresponding absorption-rate curves are shown in **Figures 3a to 3c**. In the first structure **1a** only the inner circle is present at the time the structure is resonated at different frequencies, i.e., 0.86 THz, 0.87 THz, 0.91 THz, 0.95 THz, 0.97 THz,

1.01 THz, 1.05 THz, 1.052 THz, 1.06 THz and 1.17 THz, with absorption rate of 99 %, 90 %, 99 %, 98 %, 90 %, 71 %, 92 %, 91 %, 92 %, and 85 % respectively which is shown in **Figure 1b** only the outer circle is present that time the structure is resonated at six different frequencies 0.86 THz, 0.867 THz, 0.945 THz, 0.98 THz, 1.07 THz, and 1.1 THz with absorption rate of 98 %, 90 %, 88 %, 87 %, 98 %, and 99 %, respectively, which is shown in **Figure 3b**.

3.2 Polarization (ϕ) and Angular (Θ) Stability

The projected absorption of the suggested MMA is shown in **Figures 4a** and **4b**, the oblique angles (θ) of

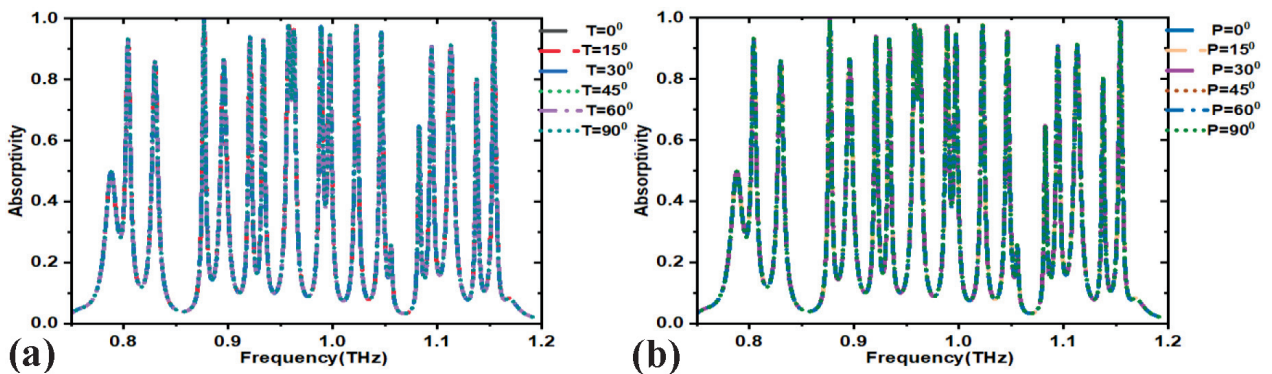


Figure 4: Absorbance characteristics of the proposed structure: a) different incident angles (θ), b) different polarization angles (ϕ), in figure, T-theta, P-Pi

the incidence and polarisation angle (ϕ) can be changed from 0° to 90° in the spectral range of interest (0.8 THz to 1.2 THz).

When the polarisation-angle and incidence-angle variables were altered, the structure's parameters such as the absorption and frequency of resonance remained constant. Consequently, the recommended MMA exhibits an excellent polarization-independent absorption capability. This is mostly due to the unit-cell uniformity of the proposed MMA. Because of the polarization-insensitive and angle-insensitive characteristics this structure finds applications in spacecraft satellite communication and polarization imaging.

3.3 Electric Field, Magnetic Field and Surface Current Distribution for Sixteen Frequencies

The physical mechanism of the MMA is analysed from the electric field, the magnetic field and the surface

current distribution plots, which are shown in **Figure 5a** [a-p], **5b** [a-p], and **5c** [a-p]. The absorber resonated at sixteen bands which are 0.80 THz, 0.83 THz, 0.876 THz, 0.895 THz, 0.92 THz, 0.93 THz, 0.957 THz, 0.962 THz, 0.988 THz, 0.997 THz, 1.02 THz, 1.04 THz, 1.09 THz, 1.112 THz, 1.137 THz and 1.154 THz. The intensity calculator, which is located alongside the distribution plots, explains the related sixteen bands' field distributions. We will distinguish which places in the picture have more field distributions and which places have fewer field distributions based on that image. **Figure 5a** shows (c, f, g, i, n, o, p) with a high electric field distribution at the dielectric's surface and across the patch resonator structure, and (a, b, d, e, h, j, k, l, m) with an electric field distribution at select points on the dielectric and patch resonator. **Figure 5b** depicts the magnetic field dispersion. The largest magnetic distribution is shown in **Figure 5b** (e, h, j, k, l, n, o, p) near the surface of the dielec-

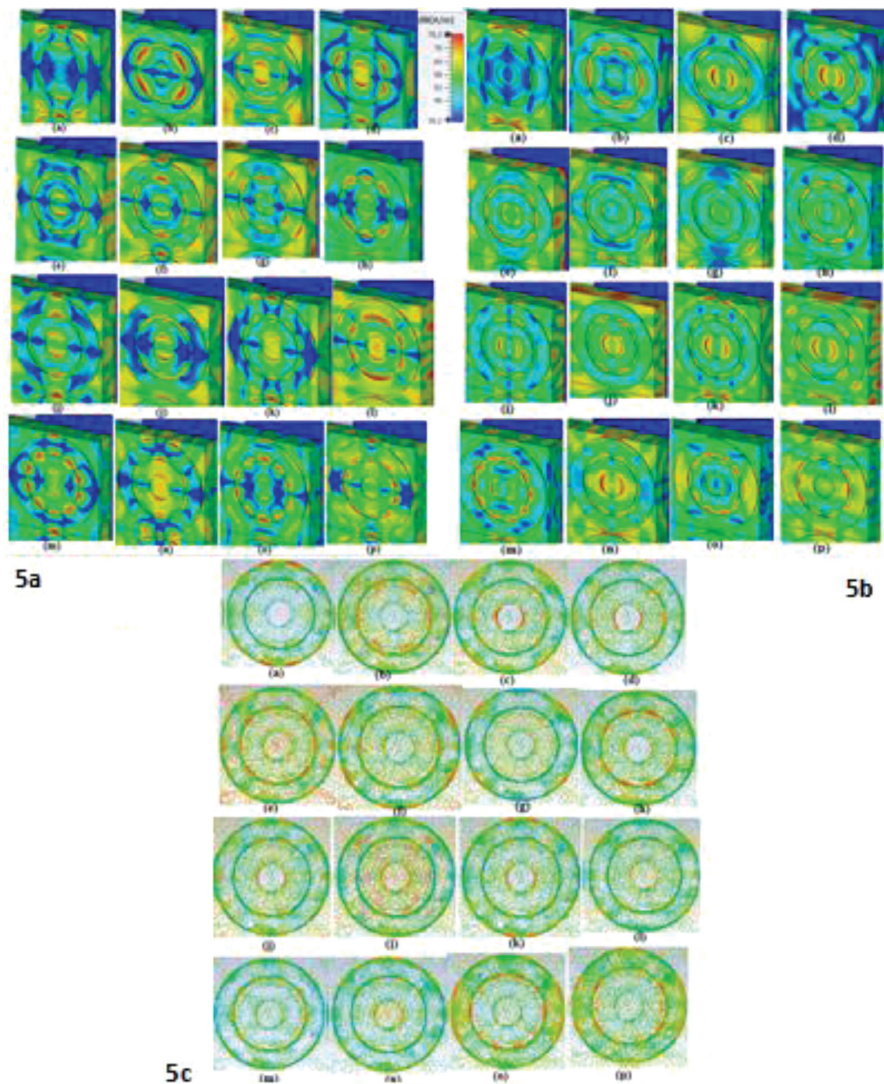


Figure 5: a) Electric field distributions, b) magnetic field distributions, c) surface current distributions: a) 0.80 THz, b) 0.83 THz, c) 0.876 THz, d) 0.895 THz, e) 0.92 THz, f) 0.93 THz, g) 0.957 THz, h) 0.962 THz, i) 0.988 THz, j) 0.997 THz, k) 1.02 THz, l) 1.04 THz, m) 1.09 THz, n) 1.112 THz, o) 1.137 THz and p) 1.154 THz

tric and across the patch resonator, whereas a little less magnetic distribution is shown in **Figure 5b** (a, b, c, d, f, g, i, m). **Figure 5c** depicts the surface-current distribution plot. The distribution of the current is greatest at the dielectric surface and the top-patch resonator structure in all the plots from a to p.

3.4 Study of design parameters

The parameter analysis assists us in determining the best absorption-rate and resonance-frequency values. Changing the parameter values results in a change in the number of bands and resonant frequencies. The goal of this effort is to achieve multiband absorption between 0.8 THz and 1.2 THz. As a result, we varied the parameters and recorded the outcomes. The graphs in **Figure 6a** and **6b** are created based on the different types of outputs with respect to the radius (R3 and R1) from the top-patch structure. First, we adjusted the outer circle R3 value from 0.12 mm to 0.20 mm in 0.2 mm steps, as shown in **Figure 5a**. At that time, we had the most bands (16), with R3 values of 0.12, 0.16, and 0.20 mm. Furthermore, we obtained fourteen bands with R3 values of 0.14 and 0.18 mm. We choose 0.16 mm as the optimal R3 value from these five distinct outputs because the absorption rate is strong at sixteen various frequencies, as shown in **Table 3**. Second, we adjusted the outer circle R1 value from 0.02 mm to 0.06 mm in 0.2 mm steps, as shown in **Figure 6b**. At that time, we had the most bands (sixteen), and the R1 value was 0.06 mm. Furthermore, we obtained eight, nine, and twelve bands with R1 values of (0.02, 0.04, and 0.05) mm, respectively. As a result of the investigation, we obtained the maximum multiband at sixteen different frequencies with the highest absorption rate.

When the outer circle radius was 0.24 mm, 0.16 mm, the resonant frequencies in the THz frequency ranges in 0.80, 0.83, 0.876, 0.895, 0.92, 0.93, 0.957, 0.962, 0.988, 0.997, 1.02, 1.04, 1.09, 1.112, 1.137, 1.154 with an absorptivity of 93 %, 86 %, 99.6 %, 86.5 %, 94 %, 93 %, 98 %, 96 %, 97 %, 95 %, 98 %, 96 %, 91 %, 91.2 %, 80 %, 99 %,

80 %, 99 % and hence 16 peaks were achieved. When the outer circle radius was 0.14, 0.06 mm, the resonant frequencies in the THz ranges in 0.80, 0.83, 0.876, 0.895, 0.92, 0.93, 0.957, 0.962, 0.988, 0.997, 1.02, 1.04, 1.09, 1.112, 1.137, 1.154 with the absorptivity of 93 %, 86 %, 99.6 %, 86.5 %, 94 %, 93 %, 98 %, 96 %, 97 %, 95 %, 98 %, 96 %, 91 %, 91.2 %, 80 %, 99 %, so 16 peaks were achieved.

When the dielectric constant and the permittivity are independently manipulated, the electric and magnetic fields could possibly be absorbed. With the help of the manipulation techniques in the reflectivity, permittivity and permeability, the impedance matching with respect to the free space can be achieved for a highly capable absorber.

3.5 Quality factor (Q-factor)

The Q value (defined as the frequency of the resonance point divided by its Full-Width Half Maximum

Table 2: FWHM and Q for sixteen resonant frequencies

Band No.	Original Frequency (THz)	Absorption (%)	FWHM	Q-Factor
1	0.80	93	0.00365	219.17
2	0.83	86	0.00471	176.22
3	0.876	99.6	0.00138	634.78
4	0.895	86.5	0.00474	188.81
5	0.92	94	0.00266	345.86
6	0.93	93	0.00255	364.70
7	0.957	98	0.00449	213.14
8	0.962	96	0.00126	763.49
9	0.988	97	0.00279	354.12
10	0.997	95	0.00243	410.28
11	1.02	98	0.0032	318.75
12	1.04	96	0.00293	354.94
13	1.09	91	0.00273	399.26
14	1.112	91.2	0.0047	236.59
15	1.137	80	0.00212	536.32
16	1.154	99	0.00225	512.88

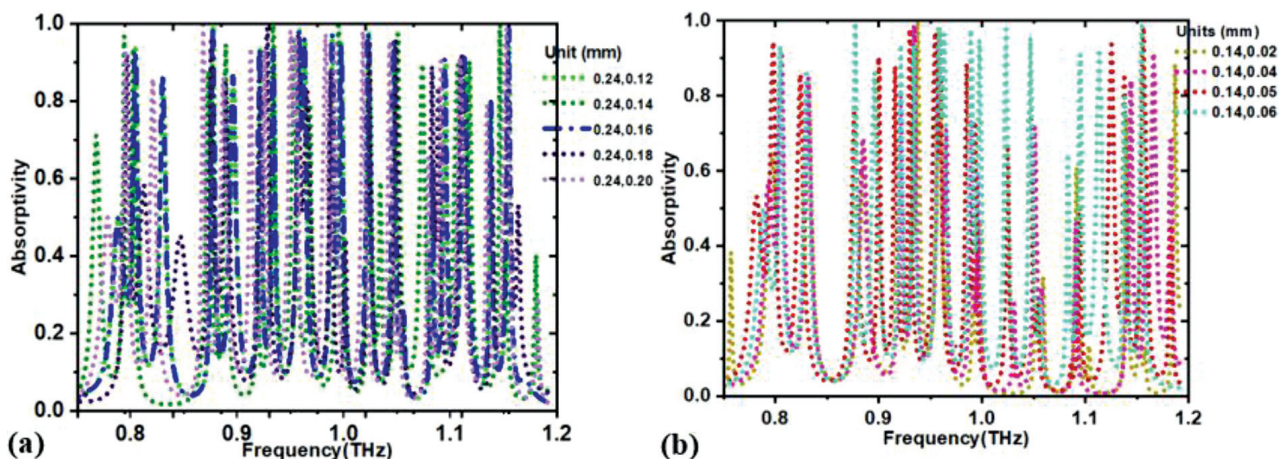


Figure 6: Absorption-curve as a function of: a) radius R3 and b) radius R1

(FWHM)) is a common parameter for deciding which frequencies to use the resonating mode on. It might be able to inform us absolutely whether the frequency selection can be used for sensing. As the Q value increases, so does the detecting capabilities.²⁰ **Table 2** shows the Q value for each frequency range, as well as a clarification of the Q value. All the frequency modes have a Q value greater than 170. When compared to the other 15 modes, the eighth mode has an extremely high Q-factor value. The sixteen-band absorber design has considerable potential in sensor-related specialty due to its high Q-factor.

4 CONCLUSION

We have created and simulated a terahertz Eight-/Nine-/Twelve-/Fourteen-/Sixteen-Band Metamaterial Absorber (MMA) for sensing applications. By varying the radius of the top-patch structure within the narrow frequency range of 0.8 to 1.2 THz, this structure generated a large number of multi bands without the use of stacked layers, numerous resonators, or overlapping in a single unit cell. By varying the angle values from 0 to 90 degrees, the polarisation and angle insensitivity properties were examined. The electric field distribution, magnetic field distribution, and surface-current distribution plots are explained to understand the internal mechanism of the proposed structure. For the sixteen-band MMA, the Q-Factor and full width half maximum are also determined. The highest value of the Q-Factor obtained from this work is 763.49. As a result, the suggested MMA will very certainly be used in biosensing and refractive-index sensing applications. This work is tabulated and compared to prior works.

5 REFERENCES

- ¹ B. Ferguson, X. C. Zhang, *Materials for terahertz science and technology*, *Nature Mater*, 1 (2002), 26–33
- ² M. Walther, B. Fischer, A. Ortner, A. Bitzer, A. Thoman, H. Helm, *Chemical sensing and imaging with pulsed terahertz radiation*, *Analytical and bioanalytical chemistry*, (2010), 397
- ³ K. Kawase, O. Yuichi, W. Yuuki, I. Hiroyuki, *Non-destructive terahertz imaging of illicit drugs using spectral fingerprints*, *Optics express*, 11, (2003) 20, 2549–2554
- ⁴ L. Yang, G. Tengxiao, Z. Xu, C. Shuya, D. Xuequan, *Toxic chemical compound detection by terahertz spectroscopy: A review*, *Reviews in Analytical Chemistry*, 37 (2018) 3, 20170021
- ⁵ L. Afsah-Hejri, A. Elnaz, T. Arash, H. Taymaz, A. Azar, E. Reza, *Terahertz spectroscopy and imaging: A review on agricultural applications*, *Computers and Electronics in Agriculture*, 177 (2020), 105628
- ⁶ R. J. Falconer, A. G. Markelz, *Terahertz spectroscopic analysis of peptides and proteins*, *Journal of Infrared, Millimeter, and Terahertz Waves*, 33 (2012), 973–988
- ⁷ T. Chen, Z. Li, X. Yin, F. Hu, C. Hu, W. Zhang, J. Han, *Classification and recognition of genetically modified organisms by chemometrics methods using terahertz spectroscopy*, *International Journal of Food Science & Technology*, 50 (2015) 12, 2682–2687
- ⁸ S. H. Baek, H. B. Lim, H. S. Chun, *Detection of melamine in foods using terahertz time-domain spectroscopy*, *Journal of agricultural and food chemistry*, 62 (2014) 24, 5403–5407
- ⁹ V. A. Trofimov, S. A. Varentsova, *A possible way for the detection and identification of dangerous substances in ternary mixtures using THz pulsed spectroscopy*, *Sensors*, 19 (2019) 10, 2365
- ¹⁰ T. J. Cui, D. R. Smith, R. Liu, *Metamaterials*. Boston, MA, USA: Springer, 2010
- ¹¹ G. V. Eleftheriades, N. Engheta, *Metamaterials: Fundamentals and Applications in the Microwave and Optical Regimes*, *Proceedings of the IEEE*, 99 (2011) 10
- ¹² T. J. Yen, W. J. Padilha, N. Fang, D. C. Vier, D. R. Smith, J. B. Pendry, D. N. Basov and X. Zhang, *Science*, 303 (2004), 1494–1496
- ¹³ E. Nader, R. W. Ziolkowski, eds. *Metamaterials: physics and engineering explorations*, John Wiley & Sons, 2006
- ¹⁴ S. Rengasamy, R. Natarajan, V. Kuttathati Srinivasan, *Miniaturized multi-spectral perfect metamaterial absorber for THz sensing, imaging and spectroscopic applications*, *Plasmonics*, 18 (2023) 2, 643–651